EARTHQUAKE ENGINEERING AND STRUCTURAL DYNAMICS, VOL. 23, 583–597 (1994)

SOURCE, PATH AND SITE EFFECTS ON DOMINANT FREQUENCY AND SPATIAL VARIATION OF STRONG GROUND MOTION RECORDED BY SMART1 AND SMART2 ARRAYS IN TAIWAN

IGOR A. BERESNEV*, KUO-LIANG WEN†, AND YEONG TEIN YEH‡
Institute of Earth Sciences, Academia Sinica, P.O. Box 1-55, Nankang, Taipei, Taiwan 11529, R.O.C.

SUMMARY

The reduction in spatial variance of strong ground motion with increasing earthquake magnitude has been reported recently. However, we show that the observed dependence of spatial variance on magnitude is its implicit dependence on the frequency content (dominant frequency) of the wave field. Time-domain cross-correlations of pairs of accelerograms are used to quantify the spatial variations in this paper. Magnitude is one of the factors contributing to the dominant frequency. We attempt to study separately the effects of magnitude, hypocentral distance, peak ground acceleration and focal depth on the dominant frequency in order to find the most significant one. The data base consists of 1965 records of horizontal acceleration from 148 local earthquakes in Taiwan. The analysis shows the overwhelming effect of the source magnitude on the formation of the dominant frequency with an empirical relationship:

$$f_D(\text{Hz}) = 19{\cdot}9 - 2{\cdot}84M_L \pm 1{\cdot}93 \quad \text{for } 3{\cdot}1 \leqslant M_L \leqslant 7{\cdot}0$$

No significant effect of hypocentral distance, local acceleration amplitude or depth is detected for all their values available (up to 170 km, 250 cm/s^2, and 100 km, respectively). The prevailing effect of magnitude on the dominant frequency is a real cause of the consistently observed reduction of spatial variance of ground motion with increasing magnitude of earthquakes.

INTRODUCTION

Nearly all published attenuation relations assume that the standard error of Peak Ground Acceleration (PGA) is constant over the range of distances and magnitudes considered.[1] However, several studies having tested this assumption revealed the dependence of spatial variation of strong ground motion on the magnitude of earthquakes, propagation distance and local acceleration. The magnitude dependence is most evident and is manifested in a general decrease of the spatial variation as magnitude increases. For instance, Sadigh[2] and Idriss,[3] who studied standard error of PGA, noted that the PGAs recorded during main shocks were less variable than the PGAs recorded during the aftershocks for the 1971 San Fernando, 1975 Oroville, 1979 Coyote Lake and 1979 Imperial Valley earthquake sequences. The similar quantitative dependence for σ_{PGA} was established by Abrahamson,[1] who used records of 25 events selected from SMART1 array data set. On the other hand, Tsai and Bolt[4] suggested that the spatial variability of PGA depends on the source radiation and propagation path effects. Donovan and Bornstein[5] use a standard error of PGA that increases with increasing acceleration. Conversely, Chin and Aki[6] suggest that the ground non-linearity can contribute to the reduction of variance in peak acceleration with increasing acceleration level.

The above studies raise the problem of the magnitude, distance, or local acceleration effect on spatial variation of ground motion, while they do not solve completely the question of its probable mechanism. It is known that a major factor controlling the spatial variance is the frequency content of the wave field. For instance, Wen and Tsai[7] found that the spatial variation of PGA increased as the frequency of the ground

*Visiting specialist.
†Associate Research Fellow.
‡Research Fellow; also Director.

CCC 0098–8847/94/060583–15

Received 22 April 1993
Revised 21 July 1993

motion increased. They based their analysis on the records of one SMART1 event (event 22). Abrahamson[8,9] and Harichandran and Vanmarcke[10] analysed spatial variations on the SMART1 array in the frequency domain using coherency functions. They also showed that for a given separation distance between stations, the value of coherency falls off with increasing frequency. Therefore, one can suppose, that the source, path or site effect on spatial variance can be primarily associated with their effect on the frequency content of the ground motion. This assumption was made by Beresnev.[11] Indeed, different authors observed the correlation between the frequency content and the magnitude of earthquakes (References 12–14). Zhou[13] showed from the analysis of local earthquakes in Sweden that the corner frequency f_{max} shifted towards lower values as earthquake magnitude increased. Caillot[14] established the same regularity for the dominant frequency using the data of three events recorded by SMART1 array (events 20, 41 and 45). Thus, the mechanism of the effect of magnitude on spatial variation proposed by Beresnev[11] consists in that larger magnitude earthquakes have more low-frequency energy that causes the reduction in spatial variance. Other factors, such as distance or acceleration, may work in the same manner through the dominant frequency of the wave field, so that to conclude about their influence on the spatial variance, one should address their effect on the frequency content of the seismic field.

A limited comparative analysis of the effects of magnitude and distance on the frequencies of ground motion recorded by the SMART1 array was done by Beresnev[11] and Roca.[12] Beresnev[11] studied the dominant frequencies using accelerograms of 18 events, while Roca[12] considered corner frequencies of 45 events. Both authors concluded that the contribution of magnitude was stronger than the contribution of distance. To our knowledge, the comparative analysis of all the factors affecting the dominant frequency including source, path and site effect using large data set was never done.

Spatial variation of strong ground motion is an important factor from the geotechnical point of view. It directly affects the seismic hazard calculation.[1,3,5] This emphasizes the importance of the study of the factors controlling the variation. In this paper we focus on the separate analysis of source, path and site effects using a full set of data available from the SMART1 and SMART2 arrays. Recordings of 148 events are used. We first consider individual examples of the dependence of spatial variation of ground motion on magnitude and dominant frequency using time-domain correlational approach to quantifying spatial variation, showing that its apparent dependence on magnitude can be explained by the relationship between magnitude and dominant frequency. We then study separate contributions of the magnitude, hypocentral distance, local acceleration, and focal depth to the dominant frequency in order to determine the most important factor. Dominant frequencies of the horizontal component of acceleration are considered in this paper. A theoretical estimate of the effect of attenuation on the dominant frequency is also given.

SMART1 AND SMART2 SEISMIC ARRAYS

SMART1 seismic array is installed in the north-east corner of Taiwan (Figure 1). It is a dense array of 39 three-component accelerographs configured in three concentric circles of radii 200, 1000 and 2000 m. All the stations are installed on recent alluvium deposits with almost uniform site conditions except for the station E-02 that is on slate outcrop. Reference 15 gives a comprehensive description of the layout and the data of SMART1 array. A geological description of the area is given by Wen and Yeh.[16] SMART1 array was operated between 10/18/1980 and 12/13/1990 and now is closed. Over this period it recorded 60 local earthquakes with the local magnitudes ranging from 3·6 to 7·0 and hypocentral distances from 2·2 to 151 km. Maximum acceleration recorded is 375 cm/sec^2. Sampling interval of all accelerograms is 0·01 sec, and the working frequency range is 0·1–25 Hz. We selected 54 events out of 60 for this analysis (Table I).

SMART2 accelerograph array[17] is located in the eastern part of Taiwan (Figure 1). It was designed to supersede SMART1 array and has been operating since 12/13/1990. SMART2 array consists of about 40 stations dispersed through the area of approximately 20 × 10 km. It does not have as regular geometric shape as SMART1; however, there is a dense subset of stations in the northern part of the array consisting of about 10 stations (Figure 1). Among them station 37 has three downhole instruments in addition to the surface one whose depths are 50, 100 and 200 m. We will use the data of only this subarray. These stations are

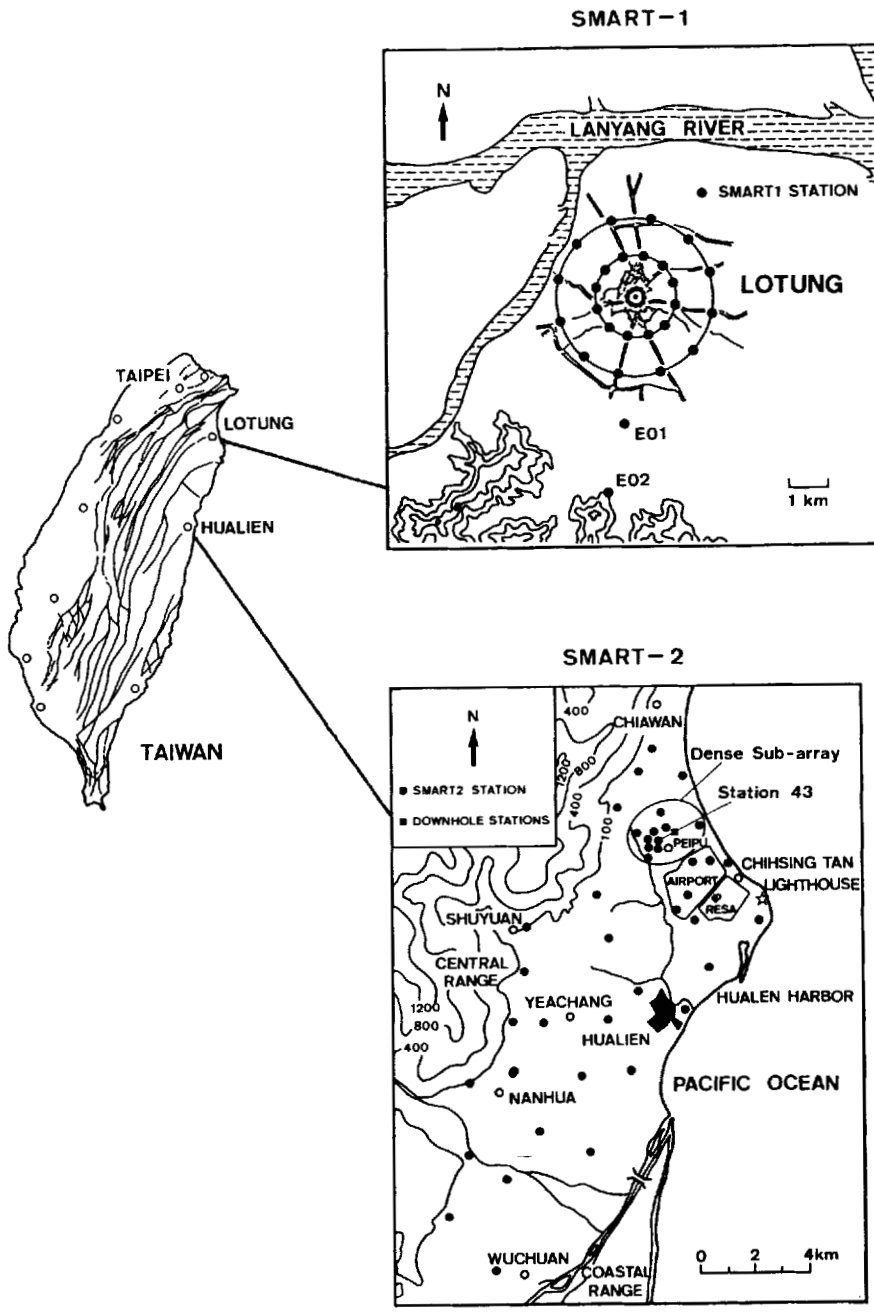

Figure 1. Location and layout of SMART1 and SMART2 arrays in Taiwan

geologically uniform and represented by Pleistocene gravel, sand and clay deposits. SMART2 array employs higher precision 16-bit instruments compared with 12-bit ones in SMART1, that ensures a better quality data. Over approximately 2 years of operation SMART2 array recorded about 200 events with local magnitudes ranging from 3·1 to 6·0 and epicentral distances up to 50 km. The maximum recorded acceleration is 317 cm/sec^2. The sampling interval is 0·005 sec, and the working frequency range is 0·1–50 Hz. Table II gives the description of the SMART2 events used in this study.

Table I. SMART1 event parameters

Event	f_D* (Hz)	σ_{f_D}† (Hz)	N‡	M_L	Depth (km)	Δ§ (km)	Δ_H‰ (km)
1	3·4	1·2	15	6·1	8·2	45·3	46·0
2	4·6	1·0	16	5·9	62·1	10·1	62·9
3	4·8	1·2	12	5·7	59·3	12·6	60·6
5	3·0	1·1	26	6·3	11·1	30·2	32·2
6	5·9	2·2	10	5·5	76·6	17·4	78·6
8	7·4	3·3	19	4·8	7·1	7·0	10·0
9	10·4	2·3	11	4·2	11·2	9·8	14·9
10	5·9	1·6	9	5·1	68·5	21·6	71·8
11	5·4	2·2	6	5·6	1·5	32·1	32·1
12	6·2	3·5	16	4·9	0·1	2·2	2·2
13	8·5	1·3	12	4·4	0·3	4·0	4·0
14	4·0	1·6	30	5·0	0·2	23·1	23·1
15	11·1	3·8	29	3·6	3·6	3·1	4·8
16	1·2	0·4	11	6·2	3·3	85·3	85·4
17	9·4	2·4	8	4·7	0·8	10·9	10·9
18	7·1	3·0	24	5·1	10·0	7·5	12·5
19	5·4	1·6	27	4·9	8·0	22·5	23·9
20	2·8	1·1	35	6·4	27·3	116·6	119·8
21	4·2	1·1	11	6·6	97·4	115·8	151·3
22	2·4	1·8	34	6·4	1·2	35·4	35·4
23	1·9	0·7	23	6·6	14·8	118·4	119·3
24	1·1	0·3	31	6·9	25·0	115·3	118·0
25	1·4	0·4	35	6·8	18·0	98·9	100·5
26	3·8	0·8	10	5·5	58·8	5·6	59·1
27	0·8	0·1	11	6·3	10·3	134·9	135·3
28	3·8	1·3	28	5·9	5·9	49·3	49·7
29	3·9	1·0	30	6·0	8·7	35·4	36·5
30	3·3	1·5	31	6·3	60·7	29·3	67·4
31	3·1	1·0	36	5·9	4·1	48·3	48·5
32	5·0	1·1	21	6·0	5·3	48·2	48·5
33	3·4	1·7	36	6·5	3·3	44·9	45·0
34	5·5	1·8	24	5·8	1·3	34·4	34·4
35	6·0	2·0	36	5·7	8·0	4·7	9·3
36	3·9	1·1	36	6·3	6·1	46·6	47·0
37	4·1	1·0	33	5·3	1·7	29·8	29·8
38	4·7	0·5	14	5·5	73·8	12·8	74·9
39	1·4	0·7	36	6·5	10·2	22·2	24·4
40	0·9	0·2	37	6·6	15·8	67·9	69·7
41	3·0	1·4	37	6·2	21·8	70·9	74·2
42	5·1	1·8	37	5·0	2·0	5·3	5·7
43	1·3	0·8	38	6·2	1·6	5·8	6·0
44	6·1	1·8	36	4·9	2·3	4·9	5·4
45	1·2	0·7	35	7·0	13·9	79·3	80·5
49	3·2	1·2	22	5·8	98·0	40·3	106·0
50	2·7	1·1	33	6·2	27·8	80·8	85·4
51	2·8	1·4	30	5·8	70·1	20·0	72·9
52	2·5	0·5	25	5·7	30·6	52·9	61·1
53	5·6	1·7	26	5·3	0·5	41·1	41·1
54	3·9	0·8	34	5·2	34·5	28·6	44·8
55	3·6	1·2	22	5·6	62·5	68·0	92·4
57	2·8	1·2	22	4·8	22·0	41·9	47·3
58	3·8	1·1	20	5·5	34·3	64·2	72·8
59	1·1	0·2	21	5·0	2·9	91·5	91·5
60	0·8	0·0	5	5·0	1·1	102·1	102·1

*Average dominant frequency.
†Standard deviation of dominant frequency.
‡Number of stations used to calculate f_D and σ_{f_D}.
§Epicentral distance from central station C-00.
‰Hypocentral distance from central staton C-00.

Table II. SMART2 event parameters

Event	f_D* (Hz)	σ_{f_D}† (Hz)	N‡	M_L	Depth (km)	Δ§ (km)	Δ_H‰ (km)
58	2·2	1·0	2	5·5	0·8	51·8	51·8
61	2·0	1·2	2	4·9	4·2	38·3	38·5
65	4·8	0·1	2	5·3	24·2	19·8	31·2
68	2·5	0·4	2	4·4	1·3	16·2	16·3
69	4·4	2·1	2	5·3	2·9	50·2	50·3
72	8·8	0·7	3	5·0	10·3	18·1	20·8
76	8·2	1·0	3	4·8	16·8	15·7	23·0
77	9·0	0·6	2	4·1	11·7	15·8	19·7
78	6·6	1·2	3	4·8	24·8	12·8	27·9
79	1·5	0·6	3	5·2	1·1	20·0	20·1
81	6·4	0·4	2	3·9	4·1	13·4	14·0
95	6·7	2·5	6	4·5	18·7	22·8	29·5
96	5·8	1·0	7	4·3	0·6	10·1	10·1
97	8·5	4·3	6	4·1	17·9	9·9	20·5
99	1·5	0·4	4	4·8	0·6	15·0	15·0
100	9·5	1·5	3	4·2	14·3	36·0	38·7
101	6·1	2·1	6	4·9	14·9	22·6	27·1
102	8·2	1·1	3	4·1	1·7	22·9	22·9
103	7·9	1·4	7	4·3	10·7	19·3	22·1
104	11·6	6·0	10	3·6	1·5	9·5	9·6
105	10·0	5·4	9	3·6	3·7	3·1	4·8
106	10·1	2·7	9	3·1	2·9	9·4	9·9
107	6·5	1·7	9	4·2	26·8	20·7	33·8
108	5·2	1·9	9	4·4	2·0	4·4	4·8
109	11·5	2·7	6	3·2	6·6	2·0	6·9
110	9·9	0·5	2	4·0	10·1	19·9	22·3
111	10·3	2·6	4	4·1	9·8	16·8	19·4
112	12·1	3·7	4	3·3	4·5	6·2	7·6
113	10·2	1·0	2	3·7	13·5	21·1	25·0
114	7·5	2·1	6	4·5	23·9	19·9	31·1
116	7·4	2·3	4	4·6	21·8	5·7	22·5
118	7·7	1·6	3	4·2	13·3	20·0	24·0
119	8·5	0·2	3	4·5	17·9	3·6	18·3
121	6·7	1·6	4	5·3	83·3	141·1	163·9
122	8·5	1·5	6	4·4	12·5	21·7	25·0
123	1·8	0·4	4	5·3	24·0	160·5	162·3
124	5·7	1·0	6	4·7	6·5	29·2	30·0
125	6·2	2·0	6	4·7	11·4	22·6	25·3
126	5·6	1·8	8	4·5	16·3	24·5	29·5
127	16·2	5·3	8	3·8	6·6	0·4	6·6
128	6·5	1·8	7	4·1	8·8	13·3	16·0
130	5·2	2·5	8	4·8	9·9	24·7	26·6
131	6·9	1·1	7	4·2	15·0	22·2	26·8
132	6·5	1·3	3	4·7	34·6	65·3	73·9
133	11·2	2·4	2	3·8	8·1	17·6	19·3
134	6·1	1·8	5	4·5	7·6	27·6	28·6
135	6·8	3·1	6	4·6	29·3	9·7	30·9
136	7·9	1·7	3	3·1	4·8	26·6	27·0
138	9·2	3·2	5	4·0	12·0	22·0	25·1
139	8·7	0·2	2	3·9	4·9	19·7	20·3
140	7·9	2·4	8	4·5	4·0	0·1	4·0
142	6·7	0·7	3	5·0	35·9	97·8	104·2
143	8·4	2·3	7	3·8	6·1	0·1	6·1
144	7·7	0·6	7	4·4	16·7	18·1	24·6
145	3·6	2·4	5	4·6	1·0	24·0	24·0
148	6·0	2·4	5	4·6	30·6	13·5	33·4

Table II. (*Contd.*)

Event	f_D* (Hz)	σ_{f_D}† (Hz)	N‡	M_L	Depth (km)	Δ§ (km)	Δ_H‰ (km)
149	6·7	1·9	5	4·1	34·3	14·9	37·4
151	17·2	2·0	4	3·5	16·1	12·9	20·6
152	8·8	1·2	8	3·9	12·1	13·2	17·9
153	7·1	0·9	5	4·6	40·7	81·0	90·7
154	6·4	1·2	6	4·0	27·4	27·1	38·5
156	5·0	2·7	6	4·9	24·5	29·2	38·1
157	6·4	1·1	8	4·3	22·3	4·1	22·7
158	7·5	0·6	3	4·8	68·0	63·6	93·1
159	13·7	7·0	3	3·3	12·6	11·0	16·7
160	3·4	2·5	4	5·5	47·2	162·8	169·5
161	6·0	1·1	9	4·9	22·6	3·9	22·9
162	7·9	0·9	6	3·7	24·8	11·0	27·1
163	4·0	2·2	7	5·0	24·2	15·6	28·8
164	7·2	0·9	6	4·4	22·1	13·7	26·0
165	6·9	1·3	6	4·4	27·3	9·4	28·9
166	11·2	2·7	3	3·3	15·5	1·8	15·6
167	11·6	2·8	7	4·6	15·3	11·9	19·4
168	4·1	1·2	7	5·7	8·4	22·5	24·0
171	6·5	1·9	7	5·0	25·0	25·9	36·0
173	4·2	2·6	7	5·1	3·3	20·9	21·2
175	6·4	2·6	7	4·7	19·0	34·6	39·5
177	8·1	2·0	9	4·5	12·6	23·0	26·2
178	6·4	1·6	10	4·3	4·6	23·8	24·3
179	8·3	0·9	3	3·2	7·3	6·3	9·6
183	4·6	1·7	11	4·8	22·7	1·0	22·7
184	12·1	3·8	11	3·8	13·4	10·1	16·8
185	5·9	1·8	11	4·8	28·6	15·2	32·4
187	4·9	2·5	11	4·9	57·8	47·7	74·9
189	6·0	1·5	8	4·8	12·8	21·5	25·0
190	4·3	1·6	11	5·1	30·0	24·1	38·5
191	4·5	1·9	11	4·6	11·7	11·6	16·5
192	5·2	1·5	11	4·8	15·7	9·0	18·1
194	1·4	0·8	11	5·2	51·4	41·4	66·0
195	11·7	5·3	8	4·1	19·1	24·2	30·8
196	0·7	0·0	6	5·8	17·6	110·8	112·2
197	5·4	2·2	7	4·9	33·2	50·7	60·6
198	12·4	2·3	8	3·6	19·0	14·3	23·8
199	6·6	2·5	12	4·8	20·2	17·4	26·7

*Average dominant frequency.
†Standard deviation of dominant frequency.
‡Number of stations used to calculate f_D and σ_{f_D}.
§Epicentral distance from central station 43.
‰Hypocentral distance from central station 43.

COMPARISON OF DEPENDENCE OF SPATIAL VARIATION OF GROUND MOTION ON MAGNITUDE AND DOMINANT FREQUENCY

Calculating characteristics of spatial variation and dominant frequencies

To show that the earlier observed magnitude dependence of spatial variation of ground motion is in fact its frequency dependence, we plot its characteristics separately against magnitude and frequency using all the data available from SMART1 array.

Spatial variation of strong ground motion can be quantified by various parameters such as the correlation or coherency. The correlation is a time-domain measure, while the coherency is a frequency-domain measure.

Coherency functions are now commonly used by engineers.[8] Calculations of frequency-dependent coherency for SMART1 data have been performed earlier.[8-10] In the studies of spatial variation dependence on magnitude, distance or acceleration, different authors used standard deviations of PGAs,[1-3] i.e. the time-domain measure. To combine these results we choose the correlation coefficient of acceleration time histories at two spaced stations as a measure of spatial variation. The pairs of stations selected in this study include the central station and the stations in the inner ring (Figure 1). The separation distance is 200 m. The wave-passage effect is present in all accelerograms due to inclined wave propagation and results in systematic shifts in the wave arrival. Triggering times of instruments do not coincide as well. To remove these effects we shift records with respect to each other to obtain their maximum correlation coefficient. Full records of the EW-component are used. To obtain a more statistically significant result, we average the obtained correlation coefficients over all available pairs.

Dominant frequencies are calculated as follows. Again, we use full records of the EW-component of ground acceleration. Their Fourier power spectra are smoothed using a three-point running Hanning average.[18] The number of smoothings is chosen experimentally considering its visual effect on the spectral shape, and it is 80 for SMART1 and 640 for SMART2 records. Dominant frequency is defined as the frequency at the maximum ordinate of the smoothed spectra. This procedure does not exclude the uncertainty in determining the dominant frequency when the spectrum is broad enough. An extreme example of such an uncertainty is given in Figure 2. Raw and smoothed spectra for one of the SMART2 accelerograms are given. The width of the EW-component spectrum is 5 to 30 Hz approximately. Smoothing changes the frequency of the maximum from 6·3 to 25·5 Hz, but all the peaks remain comparable in their magnitude. There is no significant change in the location of spectral maximum on the other components. We deliberately chose Figure 2 to show the worst case of the widest spectrum observed. Ordinarily, the uncertainty is much smaller. To minimize its influence we average calculated frequencies over a group of stations. It was the whole array in SMART1 case, and a dense subarray in SMART2 case. The hypocentral distances used in subsequent analysis were determined relative to the central station and station 43, respectively. Selected SMART2 events listed in Table II triggered at least two stations in the subarray. Note that uncertainty in the dominant-frequency (f_D) determination is reflected in the value of its standard deviation. The average f_Ds and their standard deviations are summarized in Tables I and II. One can see that the event 127 discussed above corresponds to the extremely large σ_{f_D}.

Comparison of magnitude and frequency effect on spatial variation

Figure 3 shows the average correlation coefficient of pairs of accelerograms versus local magnitude. Vertical bars indicate one standard deviation. This plot clearly shows a close-to-linear growth of the correlation with increasing magnitude. The correlation coefficient of the plotted dependence is 0·81. Event 40 has a maximum spatial uniformity (average correlation coefficient 0·94, standard deviation 0·01, magnitude 6·6, hypocentral distance 69·7 km). The maximum variability is given by earthquake 15 (average correlation coefficient 0·26, standard deviation 0·07, magnitude 3·6, hypocentral distance 4·8 km).

In Figure 4 we plot the relationship of the same correlation with an average dominant frequency of the records (in this special case we averaged frequencies over the inner ring and central station only). Horizontal bars correspond to the standard deviation in the dominant-frequency determination. Negative correlation is observed with a correlation coefficient equal to $-0{\cdot}74$. Comparison of Figures 3 and 4 demonstrates that larger magnitudes are associated with lower frequencies, so that spatial variance decreases with increasing magnitude or decreasing frequency. This fact suggests that the frequency content, not the magnitude, is responsible for the degree of spatial variance of surface accelerations. The somewhat smaller absolute value of the correlation between quantities plotted in Figure 4 with respect to that in Figure 3 (0·81 versus 0·74) is probably explained by the fact that the dominant frequency does not characterize entirely the actual frequency content of the wave field. This is reflected in the standard deviations plotted in Figure 4. Nonetheless, the tendency of the variance to be reduced with decreasing frequency is clear. Plots illustrating direct relationship between the dominant frequency and magnitude are discussed in the next section.

For the sake of comparison of the time-domain and frequency-domain approaches to quantifying spatial variations, we emplaced the coherency function on the same plot in Figure 4. This curve is the absolute value

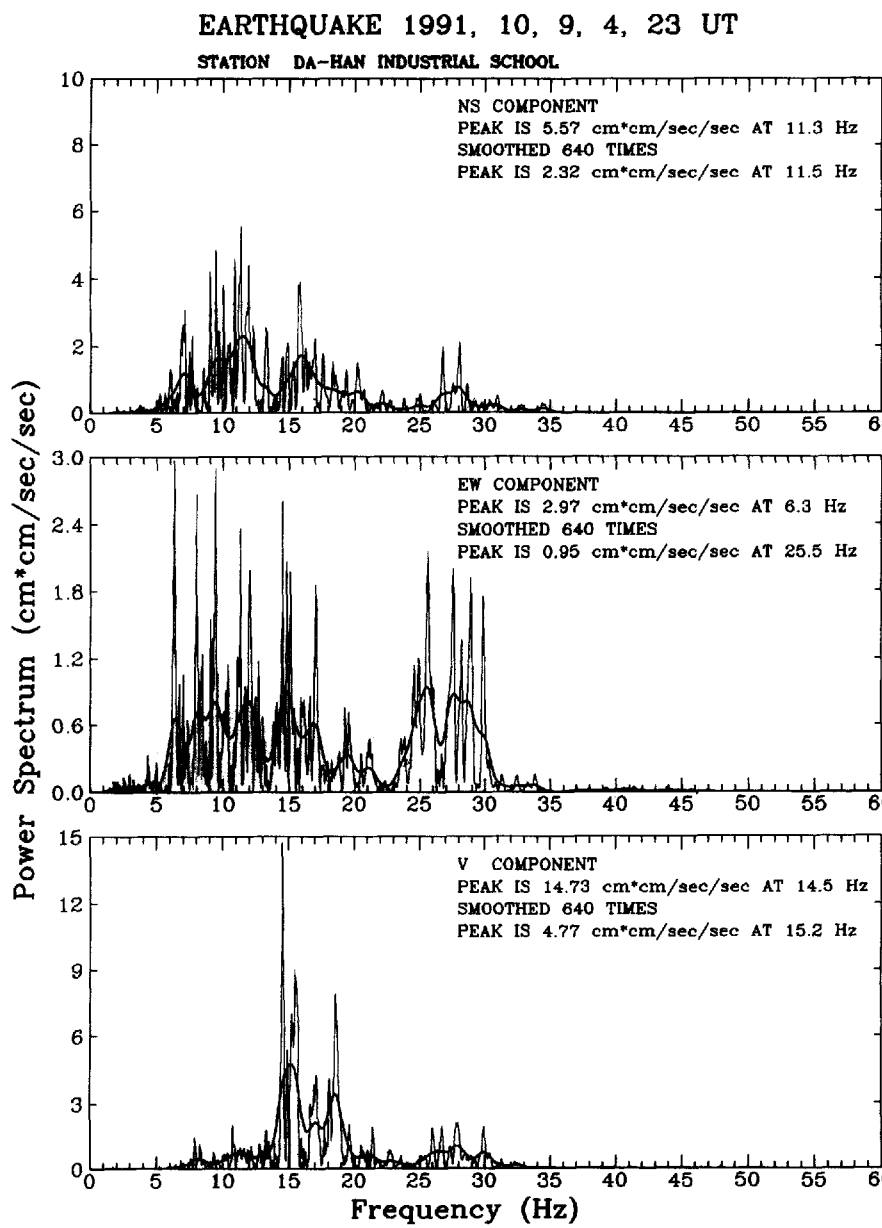

Figure 2. Raw and smoothed power spectra of one of the SMART2 records (event 127)

of coherency for SMART1 event 45 and same separation distance of 200 m, given by Abrahamson.[9] According to Abrahamson,[8] coherency is defined by a complex number

$$\gamma_{jk}(f) = \frac{S_{jk}(f)}{[S_{jj}(f)S_{kk}(f)]^{1/2}}$$

where f is the frequency and $S_{jk}(f)$ is the smoothed cross-spectrum. The smoothed cross-spectrum is given by

$$S_{jk}(f_n) = \sum_{m=-M}^{M} W_m u_j(f_{n+m}) u_k(f_{n+m})$$

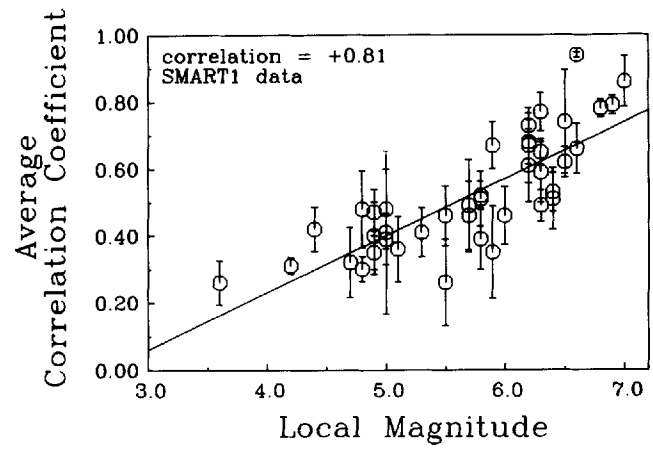

Figure 3. Dependence of the average correlation coefficient of the acceleration time histories of the central station and stations in the inner ring of SMART1 array on magnitude. The separation distance is 200 m

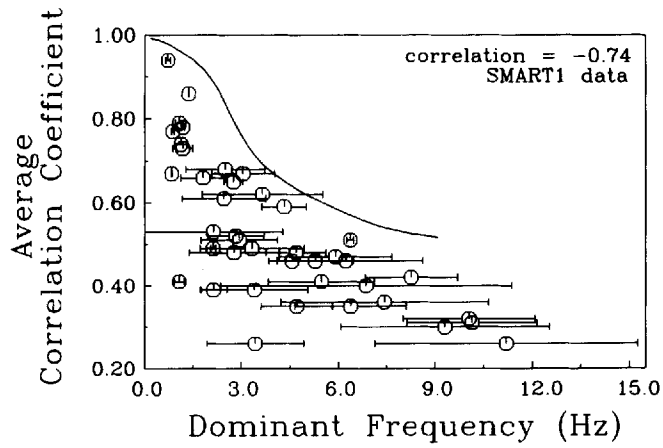

Figure 4. Dependence of the correlation coefficients shown in Figure 3 on the dominant frequency of earthquakes. Solid line is the coherency function adapted from Abrahamson[9]

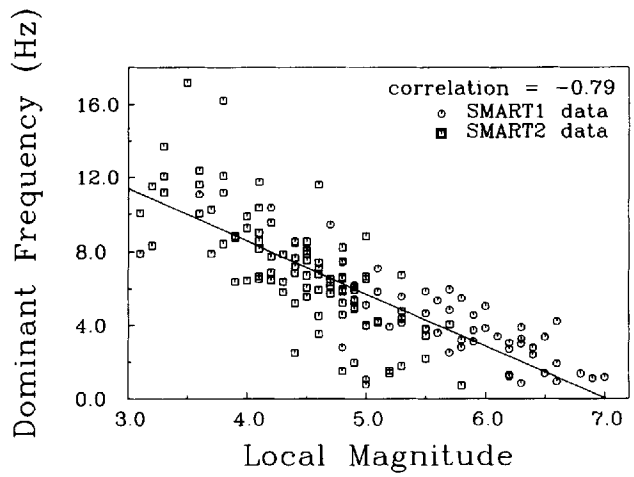

Figure 5. Dependence of the average dominant frequency of ground motion on magnitude. Solid line is a linear regression

where $u_j(f)$ is the Fourier spectrum at station j, W_m is the frequency window function, and M is a smoothing parameter defining the frequency band in which the similarity of spectra is assessed. The modulus of coherency $|\gamma_{jk}(f)|$ takes the values between -1 and 1 and does not contain the wave-passage effect, so it is directly comparable to the correlation coefficients given in Figure 4. Comparison shows that although the general trend to the lower values with increasing frequency is remarkably consistent in both cases, the coherency function lies above correlation coefficients for all frequencies. However, this is not a surprising result. Abrahamson[8,9] points out that the selection of the smoothing parameter M is critical in the estimation of coherency. In Reference 9 he shows that $|\gamma_{jk}(f)|$ rapidly decreases as M increases. Coherencies shown in Figure 4 correspond to a 2 Hz bandwidth. As for correlation coefficients, they are calculated in the time domain and thus correspond to a full bandwidth of the accelerogram. One can expect therefore that the increase in M would reduce coherency values to the values of the correlation coefficients given in Figure 4. Consequently, these two approaches give the same conclusion about the spatial variation decrease with increasing frequency.

COMPARATIVE ANALYSIS OF THE FACTORS CONTRIBUTING TO THE DOMINANT FREQUENCY OF GROUND MOTION

The above analysis shows that to understand source, path or site effect on spatial variance of ground motion one should consider their effect on the dominant frequency.

A comparison of Figures 3 and 4 demonstrates that larger magnitude earthquakes have more significant relative contributions of low-frequency energy. However, it cannot be considered as final evidence that magnitude governs the frequency content of the wave field unless we consider another factor. Ordinarily, strong motion data show positive correlation between magnitude and distance. It may happen, therefore, that the dominant-frequency dependence on magnitude is its implicit dependence on distance, since larger magnitude events are more distant and may have lower dominant frequencies due to attenuation.

Figure 5 shows the dependence of the average dominant frequency on the magnitude for a set of 148 events recorded by both arrays. Standard deviations of calculated frequencies can be found in Tables I and II. SMART1 and SMART2 data are consistent in the sense that there is no systematic deviation of calculated frequencies on one array relative to another, despite there being a difference in working frequency range, instrument type and soil conditions. SMART1 data cover mostly the high-magnitude range, while SMART2 data are indispensable to cover the low-magnitude one. Dominant frequency evidently decreases as magnitude of the earthquake increases, which accounts for the reduction of spatial variation with magnitude shown in Figure 3. The correlation coefficient of the entire dependence is $-0{\cdot}79$. SMART1 earthquake 40 having minimum variance in Figure 3 has an average dominant frequency of 0·92 Hz, while earthquake 15 that demonstrates a maximum variance has a frequency of 11·1 Hz. The frequency decline with magnitude is approximated by a linear regression law

$$f_D(\text{Hz}) = 19{\cdot}9 - 2{\cdot}84M_L \pm 1{\cdot}93 \quad \text{for } 3{\cdot}1 \leqslant M_L \leqslant 7{\cdot}0 \tag{1}$$

The ambiguity in estimating the dominant frequency for the broadband events as well as uncertainty in magnitude estimation may be the causes of the observed scattering of the data around the solid line.

Interestingly, deeper earthquakes show a better correlation of the dominant frequency and magnitude. In Figure 6 we show the frequency–magnitude dependence for the earthquakes having a focal depth more than 10 km. The data set has been reduced to 90 points. The new value of the correlation coefficient is -0.85. The equation of the linear regression changes to $f_D(\text{Hz}) = 21{\cdot}2 - 3{\cdot}05M_L \pm 1{\cdot}66$.

As mentioned earlier, there has been a doubt that the apparent dominant-frequency dependence on magnitude is not an artifact caused by the magnitude–distance positive correlation. In particular, this correlation has been reported in References 1, 19 and 20. It means that stronger earthquakes are usually more distant and are more strongly affected by attenuation. However, Abrahamson[1] showed that the standard deviation of PGA was better correlated with magnitude than with distance. Beresnev[11] and Roca[12] compared the contribution of magnitude and distance to the frequency content and also concluded that the magnitude factor was more significant. We check the contribution of the hypocentral distance to the dominant frequency using the full SMART1 and SMART2 data set.

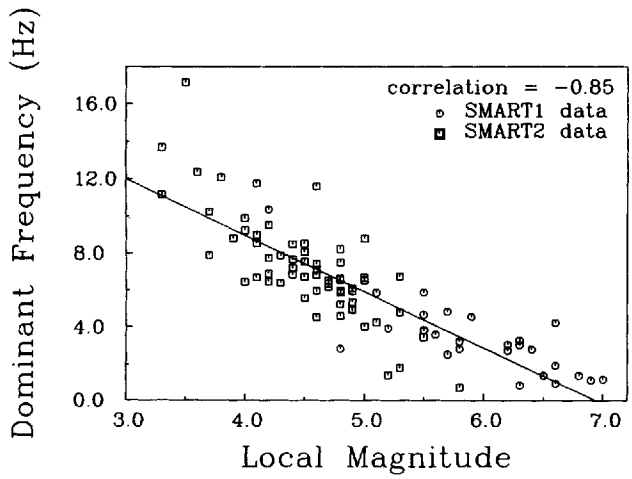

Figure 6. Dependence of the average dominant frequency of ground motion on magnitude for the events with a focal depth $\geqslant$ 10 km. The corresponding subset of 90 events from Figure 5 is shown

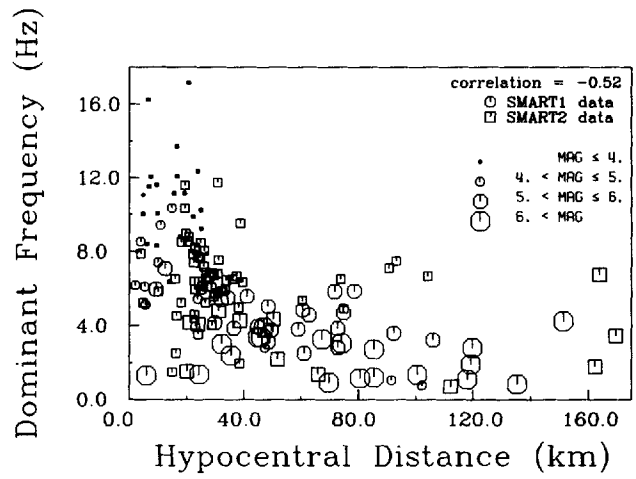

Figure 7. Dependence of the average dominant frequency of ground motion on hypocentral distance. The same events as in Figure 5 are used

Figure 7 is a 'dominant-frequency–distance' dependence for the same events shown in Figure 5. Evidently, if the dependence of f_D on magnitude is its latent dependence on distance one should find its better correlation with distance. However, Figure 7 does not show any correlation up to the distances of approximately 40 km. In Figure 7 the larger magnitude events are marked by a larger symbol size. The farthermost events are not associated with the lowest frequencies. On the contrary, small-magnitude events are shifted to the top and large-magnitude ones to the bottom of the plot. The overall correlation coefficient is $-0{\cdot}52$ versus $-0{\cdot}79$ in Figure 5. An apparent fall-off of the frequency at the distances greater than 40 km is most probably caused by the scarcity of low-magnitude data recorded in this range.

Figure 7 demonstrates no effect of attenuation on the dominant frequency in the hypocentral distances range available from our data set. This result must be consistent with the theoretical estimate of the attenuation-induced shift in the dominant frequency, based on the observed dissipative properties of the earth's crust. Such an estimate is given in the next section.

We also check the effect of local acceleration on the dominant frequency of ground motion. Dominant frequencies of 1407 individual records of 57 SMART1 events are plotted as a function of their peak acceleration in Figure 8. Larger circles correspond to the records of the rock site station E-02. The overall

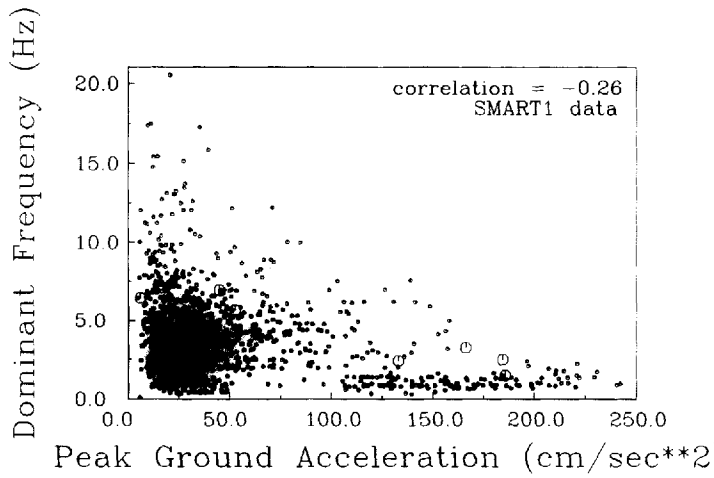

Figure 8. Dependence of the average dominant frequency of ground motion on peak ground acceleration

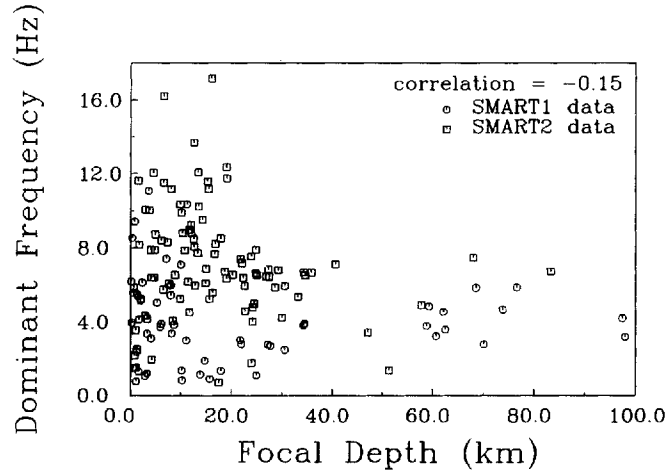

Figure 9. Dependence of the average dominant frequency of ground motion on the focal depth of earthquakes. The same events as in Figure 5 are used

correlation coefficient is −0·26. There is no visible correlation between the frequency and PGA level in the acceleration range between 0 and approximately 50 cm/sec^2. Again, the apparent decrease of f_D for higher accelerations may be caused by a lack of data in this range. This result evinces that the values of peak acceleration do not affect the formation of the dominant frequency. There is also no systematic difference between the rock and soft alluvial sites.

Finally, we check the influence of the focal depth on the dominant frequency. We demonstrated earlier that the correlation of the dominant frequency with magnitude was better for deeper earthquakes than for the shallow ones. It may be suggestive of the general relationship between frequency and depth. However, it is not so. Figure 9 gives the plot of f_D as a function of focal depth. The correlation coefficient has a trifling value of −0·15.

THEORETICAL CALCULATION OF THE EFFECT OF ATTENUATION ON DOMINANT FREQUENCY

Figure 7 demonstrated unimportance of the effect of distance, and then attenuation, on the dominant frequency relative to the magnitude effect in the hypocentral distances range considered. The more accurate assertion about the extent of the effect of distance can be done using a quantitative approach.

The path effect in Figure 5 can be manifested in the shift of the dominant frequency to the lower values for the events that have larger hypocentral distance relative to the events that have the same magnitude and are closer to the array. Generally speaking, this effect may cause observed scattering of the data around the regression line. A reasonably accurate estimate of such a shift for a given propagation distance can be done as follows.

Let us approximate the source spectrum near its maximum by a 'bell-shaped' curve

$$S(\omega) = e^{-[(\omega-\omega_D)/\sigma]^2}$$

where ω_D is the frequency of the maximum, σ characterizes the spectrum width and peak amplitude is assumed to be unity. In the presence of attenuation, the spectrum at distance L is

$$S(\omega, L) = e^{-[(\omega-\omega_D)/\sigma]^2} e^{-\alpha(\omega)L} \tag{2}$$

where $\alpha(\omega)$ is the attenuation coefficient. The frequency of the maximum in equation (2) will shift compared with ω_D. To calculate the new frequency, we take a derivative of equation (2) with respect to ω and equate it to zero

$$S'_\omega(\omega, L) = -S(\omega, L)\left[2\left(\frac{\omega-\omega_D}{\sigma^2}\right) + \alpha'(\omega)L\right] = 0$$

This gives an equation to determine a new frequency of the maximum

$$2\left(\frac{\omega-\omega_D}{\sigma^2}\right) + \alpha'(\omega)L = 0 \tag{3}$$

Now it is convenient to work in terms of a quality factor Q and frequency f. We use the definition of Q from

$$\alpha(\omega) = \frac{\omega}{cQ(\omega)}$$

where c is a wave velocity. Equation (3) becomes

$$(f-f_D) + \frac{L\sigma^2}{4\pi cQ(f)}\left[1 - \frac{fQ'(f)}{Q(f)}\right] = 0 \tag{4}$$

Let us assume Q in the form

$$Q(f) = Q_0 f^n \tag{5}$$

where Q_0 and n are constants. After substituting equation (5) into equation (4), we obtain a final form of the equation for a new frequency of the maximum

$$(f-f_D) + \frac{(1-n)\sigma^2 L}{4\pi Q_0 c} f^{-n} = 0 \tag{6}$$

By solving the algebraic equation (6) numerically, we can estimate the deviation of the dominant frequency from its initial value f_D caused by the frequency-dependent Q in Northern Taiwan. Observed dependencies $Q(f) = Q_0 f^n$ valid up to the frequency of 10 Hz are summarized by Wang.[21] In calculations we use $f_D = 8$ Hz, $\sigma = 5$ Hz, $L = 160$ km. We take a value of $c = 3600$ m/sec characteristic of the average shear wave velocity in the depth interval 0–80 km given by the one-dimensional crust model beneath Taiwan.[22] The maximum shift $f_{NEW} - f_D = -0{\cdot}04$ Hz is given by the dependence $Q = 117f^{0{\cdot}77}$ that is the coda Q from Reference 23. This value is small compared with the standard deviation of the data points in Figure 5. Thus, the theoretical change in the dominant frequency due to the path effect is in accordance with the observed data. They show no effect of attenuation on the dominant frequency.

DISCUSSION

We have studied the dependence of the dominant frequency of strong seismic motion on the factors characterizing source, path and site effect contribution such as local magnitude, propagation distance, focal

depth and peak acceleration. The importance of this study is connected with the fact that the dominant frequency is a major factor determining the degree of spatial variance of ground motion.

An analysis of the records of 148 events of SMART1 and SMART2 dense arrays (a total of 1965 individual records) showed the overwhelming effect of source magnitude on the formation of the dominant frequency. The correlation coefficient characterizing the dependence of the dominant frequency averaged over many stations on local magnitude is $-0{\cdot}79$. It decreases to a negative value of $-0{\cdot}85$ for the events with a depth of more than 10 km. Despite many authors indicating that such an effect may be a hidden form of the dominant-frequency dependence on the propagation distance, we did not observe such an artifact in our data. There are two arguments for it. First, the correlation coefficient of the frequency–distance dependence is only $-0{\cdot}52$. Second, theoretically estimated shift of the dominant frequency due to the influence of attenuation along the propagation path has a negligibly small value. Therefore, we conclude that the source effect prevails over the path effect in the formation of the dominant frequency of seismic waves. This is true at least for the hypocentral distances of up to 170 km considered in this analysis and in the geological setting of Northern Taiwan. However, we deem that this effect has a more global character.

A remarkable feature shown in Figure 5 is that the frequency values calculated from SMART1 and SMART2 arrays, which are characterized by different soil conditions, do not exhibit any systematic deviation from each other. This indicates that possible differences created by dissimilar soil characteristics are much less than the effect produced by the difference in magnitudes, so that these data can be combined together in the derivation of the empirical formula (1).

Our analysis also showed that there is no visible effect of the local acceleration amplitude on the formation of dominant frequency. This can suggest that the ground non-linearity does not affect substantially the formation of acceleration spectra, at least their dominant frequency, or this influence is suppressed by the source effect.

Chin and Aki[6] and Yu *et al.*[24] argue that the reduction of variance in peak acceleration with increasing magnitude of earthquake is probably explained by the site non-linearity. However, we show that this is caused by the decrease in the dominant frequency with magnitude, i.e. the source, not site, effect. However, non-linearity can also play a certain role. Namely, recent experimental and theoretical investigations show that it can reduce the soil amplification factor.[6,24–27] This can be considered as another mechanism controlling spatial variation which is a true site effect. It probably is of minor importance compared with the effect of the dominant frequency, but its contribution may become significant in the high-acceleration range.

The mechanism of the reduction in the dominant frequency of earthquakes with increasing magnitude is not clear enough. Increase of the magnitude may be accompanied by the growth of the source area that causes the reduction in dominant frequency. On the other hand, it can also be caused by the non-linear elastic wave effects in the source itself. For instance, numerical simulation of the non-linear wave equation near the source[28] shows that non-linearity creates the energy at zero and near-to-zero frequencies. This effect becomes stronger with increasing wave amplitude. Experimental verification of this phenomenon is worthy of special investigation.

ACKNOWLEDGEMENTS

We wish to thank Dr. H.-C. Chiu and the technical staff of the Institute of Earth Sciences who are responsible for the operation of SMART2 array. The corrected accelerograms were prepared by Mr. W. G. Huang and the data processing group. We are grateful to two reviewers who suggested a significant improvement of the paper. This work was supported by the National Science Council, R.O.C. under the grant NSC 82-0202-M-001-132.

REFERENCES

1. N. A. Abrahamson, 'Statistical properties of peak ground accelerations recorded by the SMART1 array', *Bull. seism. soc. Am.* **78**, 26–41 (1988).
2. K. Sadigh, 'Considerations in the development of site-specific spectra', in *Proc. Conf. XXII, A Workshop on Site Specific Effects of Soil and Rock on Ground Motion and Their Implications for Earthquake-Resistant Design*, Santa Fe, New Mexico, 1983, *U.S. Geol. Surv., Open-File Report 83-845*, 1983, pp. 423–458.

3. I. M. Idriss, 'Evaluating seismic risk in engineering practice', in *Proc. 11th intl. conf. on soil mech. and foundation eng.*, San Francisco, California, 1991, pp. 255–320.
4. Y. B. Tsai and B. A. Bolt, 'An analysis of horizontal peak ground acceleration and velocity from SMART1 array data', *Bull. inst. earth sci. acad. Sin.* **3**, 105–126 (1983).
5. N. C. Donovan and A. E. Bornstein, 'Uncertainties in seismic risk procedures', *J. geotech. eng. div. ASCE* **104**, 869–887 (1978).
6. B.-H. Chin and K. Aki, 'Simultaneous study of the source, path, and site effects on strong ground motion during the 1989 Loma Prieta earthquake: a preliminary result on pervasive nonlinear site effects', *Bull. seism. soc. Am.* **81**, 1859–1884 (1991).
7. K.-L. Wen and Y. B. Tsai, 'The behavior of the ground motion and source parameters from SMART1 array analysis of the May 10, 1983 Taipingshan earthquake', *Bull. inst. earth sci. acad. Sin.* **5**, 87–114 (1985).
8. N. A. Abrahamson, 'Spatial coherency of ground motion from the SMART1 array', *Geotechnical news* **9**, 31–34 (1991).
9. N. A. Abrahamson, 'Empirical models of spatial coherency of strong ground motion', in *Proc. 2nd workshop on strong motion arrays*, Taipei, Taiwan, 1988, pp. 65–92.
10. R. Harichandran and E. Vanmarcke, 'Space–time variation of earthquake ground motion', *Research Report No. R84-12*, Department of Civil Engineering, Massachusetts Institute of Technology, Cambridge, MA, 1984.
11. I. A. Beresnev, 'Spatial coherency of the strong ground motions on the SMART1 seismic array', in Institut für Bodenmechanik und Felsmechanik, Universität Karlsruhe (eds), *Soil Dynamics and Earthquake Engineering V*, Computational Mechanics Publications and Elsevier Applied Science, Southampton and Boston, 1991, pp. 99–107.
12. A. Roca, 'F_{max} dependence on source parameters analyzed from SMART-1 accelerograms (abstract)', in *XX General Assembly of IUGG, Book of Abstracts of IASPEI*, Vienna, Austria, 1991, p. 128.
13. Y.-P. Zhou, 'F_{max} observed in Northern and Central Sweden (abstract)', in *XX General Assembly of IUGG, Book of Abstracts of IASPEI*, Vienna, Austria, 1991, p. 128.
14. V. Caillot, 'Quantification Statistique et Etude Expérimentale de Mouvements Sismiques. Application à l'Evaluation du Risque', *These de Docteur*, Observatoire de Grenoble et Institut de Recherches Interdisciplinaire de Géologie et de Mécanique, Grenoble, France, 1992, pp. 36–39.
15. N. A. Abrahamson, B. A. Bolt, R. B. Darragh, J. Penzien and Y. B. Tsai, 'The SMART 1 accelerograph array (1980–1987), a review', *Earthquake spectra* **3**, 263–287 (1987).
16. K.-L. Wen and Y. T. Yeh, 'Seismic velocity structure beneath the SMART1 array', *Bull. inst. earth sci. acad. Sin.* **4**, 51–72 (1984).
17. H.-C. Chiu and Y. T. Yeh, 'A new strong-motion array in Taiwan—SMART2 (abstract)', in *XX General Assembly of IUGG, Book of Abstracts of IASPEI*, Vienna, Austria, 1991, p. 132.
18. E. R. Kanasewich, *Time Sequence Analysis in Geophysics*, The University of Alberta Press, Winnipeg, Canada, 1981, p. 456.
19. D. M. Hadley, D. V. Helmburger and J. A. Orcutt, 'Peak acceleration scaling studies', *Bull. seism. soc. Am.* **72**, 959–979 (1982).
20. Y. Fukushima and T. Tanaka, 'A new attenuation relation for peak horizontal acceleration of strong earthquake ground motion in Japan', *Bull. seism. soc. Am.* **80**, 757–783 (1990).
21. J. H. Wang, 'Q values of Taiwan: a review', *J. geol. soc. China* **36**, 15–24 (1993).
22. S. W. Roecker, Y. T. Yeh and Y. B. Tsai, 'Three-dimensional P and S wave velocity structures beneath Taiwan: deep structure beneath an arc-continent collision', *J. geoph. res.* **92**, B10, 10547–10570 (1987).
23. K. C. Chen, T. C. Shin and J. H. Wang, 'Estimates of coda Q in Taiwan', *Proc. geol. soc. China* **32**, 339–353 (1989).
24. G. Yu, J. G. Anderson and R. Siddharthan, 'On the characteristics of nonlinear soil response', *Bull. seism. soc. Am.* **83**, 218–244 (1993).
25. M. Sugito and H. Kameda, 'Nonlinear soil amplification model with verification by vertical strong motion array records', in *Proc. fourth U.S. nat. conf. on earthquake eng.*, Palm Springs, California, Vol. 1, 1990, pp. 555–564.
26. K. Aki, 'Local site effects on weak and strong ground motion', *Tectonophysics* **218**, 93–111 (1993).
27. K.-L. Wen, 'Non-linear soil response in ground motions', *Earthquake eng. struct. dyn.* **23**, 599–608 (1994).
28. I. A. Beresnev, 'Numerical model of the spherical elastic wave propagation in a nonlinear medium', *Int. j. modern phys. C (phys. comput.)* **2**, 250–253 (1990).